Thermophysics and Aeromechanics, *2019*, *Vol. 26*, *No. 3*

DOI: 10.1134/S0869864319030077

Liquid atomization in a high-speed coaxial gas jet*

V.M. Boiko, A.Yu. Nesterov, and S.V. Poplavski

Khristianovich Institute of Theoretical and Applied Mechanics SB RAS, *Novosibirsk*, *Russia*

E-mail: bvm@itam.nsc.ru, s.poplav@itam.nsc.ru

(*Received December 10*, *2018*; *revised January 30*, *2019*; *accepted for publication February 28*, *2019*)

The paper studies the process of liquid atomization in high-speed gas jets with application to a subject of high-rate fuel nozzles. Experiments were carried out for gas-liquid jet with the central-axis feeding of liquid to the outlet of a confuser-type nozzle with pumping of air in subsonic and supersonic flow regimes. The energy balance approach was developed for describing a gas-liquid jet. This provided us the needed data for comprehensive description of the gas-liquid jet: gas velocity field without liquid, shadow visualization of geometry and wavy structure of a jet with liquid and with pure gas, velocity profiles for liquid phase, spray droplet size, spray concentration and spatial distribution. The gas-liquid flow was characterized by Weber number from the time of liquid jet breakup till the final spray.

Keywords: high-speed jet, gas-droplet flow, droplets aerobreak.

Introduction

Different methods of atomization (dispersion) applied to liquids are widely used in traditional technologies, but also find applications in innovations, like state-of-art firefighting tools, chemicals spraying and coating for machinery parts, pharmaceuticals, medical sprays, industry-scale air cleaning, and heat transfer in microelectronics. The most important applications are the fuel nozzles in aviation and space engines as well as high-rate gas-liquid nozzles used for complicated rheology fluids. The latter case of nozzles is widely used in energy industry and oil industry. However, the spraying processes remain not properly studied, especially for the operation ranges critical for those technologies. This is true for the modes with supersonic gas flow. Besides the liquid atomization [1–7], we face a lot of physical processes: velocity relaxation of phases [3–5, 8, 9], droplets interaction with shocks, interphase heat transfer, phase transitions and coagulation [1, 2]. Moreover, the transfer processes of that kind can be found in natural atmospheric phenomena, e.g., in thunder-cloud fronts. In smaller scale, they are observed in a gas turbine [10]. Here we foresee another fundamental feature in study of gas-liquid flows — the problem of scaling-up of lab results. The modern technologies dictate another motivation for systematic research in the field of gas-liquid flows. The progress in numerical simulation of aero-induced liquid atomization was observed in recent years. This seems

* Research was supported by the Program for fundamental research by the state academies of sciences for 2013–2020 years (project AAAA-A17-117030610137-0).

to be a fundamental tool for forecasting of behavior of complex two-phase gas-dynamic systems. However at present, most of simulation results need comprehensive validation. The systematic experimental data on gas-liquid flow structure obtained with reliable and proofed methods are of great demand for verification of numerical models developed for liquid atomization in gas flows [11, 12].

Thus, the research of non-equilibrium gas-liquid systems shows importance even beyond technical applications. Experimental study of liquid atomization and behavior of spays in gas flows with gradients is an important fundamental problem of multiphase heat and mass transfer in non-equilibrium heterogeneous systems.

1. Gas-liquid jets and secondary breakup of droplets

There exist many technical applications using pneumatic high-rate nozzles (~1 m^3/h), for example, in situations of waste fuel flaring during well testing (to avoid oil spills with environmental damage). In focusing on fuel combustion problem, the pneumatic nozzle efficiency is determined both by quality of fuel atomization and sufficient input of oxidizer to the sprayed fuel; this supply can be achieved either through the nozzle or through air ejection from the ambient space. The modern technology offers pneumatic nozzles of *Y*-jet type [13] as most efficient solution for high-rate atomization. Here the primary liquid jet breakup occurs in the mixing chamber (in a prechamber) with the impact from the lateral gas jets, meanwhile the secondary droplet breakup occurs during mixture ejection from the nozzle. The key factor of droplet breakup beyond the nozzle is the velocity delay from the gas flow. This process can be covered in several stages: the offspring droplets is not a final result, but they keep splitting down the stream due to velocity difference between two phases. This situation takes place in the gradient-type stream; however, there were no comprehensive studies on droplet behavior in those streams. Most of experimental data on secondary droplet breakup were obtained for quasi-stationary flows behind the shock waves or for uniform flows. Those data have been classified according to the Webber number (We) [1, 2, 5–7]. Typically, this approach was used not only for original steady flows, but also (lack of alternative data) to other flow configurations: droplet injection into a vortex wake [10], cross-flow injection of a droplet chain into a stream [14], and for all types of gas-liquid jets [11–13, 15, 16]. In this paper, we also take the widely accepted flow classification by the We number, but first we focus on the problem of liquid jet instability as the primary source of droplets.

Typically, two limiting cases of liquid jet instability are considered [16]: the first case is a liquid jet in steady gas, while the second is liquid in a gas jet. The first limiting case originates back to research performed by Plateau and Rayleigh (in 1873 and 1879): the jet decays into fragments with the lengths (~$4D_l$) being close to the highest wavelength of surface instability for a jet. Here the surface tension breaks up the jet. This case is known as "thin jet" approximation and it works for the range of $\mathrm{Re}_l = \rho_l u_l D_l / \mu_l \le 100$, where ρ_l, u_l, and μ_l are the density, velocity, and dynamic viscosity of liquid, and D_l is the jet diameter [16].

For the coaxial gas jet (the second variant), the jet decay nature is different: a conjugated boundary layer is formed below the liquid surface. This is a place for the development of Kelvin–Helmholtz (KH) instability with waves generated at the interface. The wave growth and wave stripping defines the average droplet size in the spray; this size is two orders lower than the size of droplets produced by Plateau–Rayleigh mechanism [16]. The subject of this study is the aero-induced liquid atomization with appropriate governing parameters — numbers We, Re, etc.

The Weber number We is the ratio of the disturbing force from the flow onto the droplet $\sim\rho u^2 d^2$ to the droplet-stabilizing force of surface tension $\sim\sigma d$, therefore, we have the ration $\mathrm{We} = \rho u^2 d / \sigma$, where ρ and u are the density and velocity of gas flow, d and σ are the size of droplet and surface tension of liquid [1, 2, 5–7]. In case of jets, we substitute parameter d with

the jet diameter D_l. The morphology features create the classification for droplet shuttering [1, 2, 5].

1. Vibrational breakup: $8 < We < 12$.
2. Bag breakup: $12 < We < 50$.
3. Bag-and-stamen breakup: $50 < We < 100$.
4. Stripping of a boundary layer from the droplet equator (sheet stripping): $100 < We < 350$.
5. Wave crest stripping: $350 < We < 10^3$.
6. Catastrophic breakup: $We > 350$.

The other classifications of breakup process are available: they may be different in the boundaries for critical Weber numbers We_{cr} or (more importantly) in interpretation of the same observations. Herein we add some comments on this classification: they might be important for the secondary droplet breakup after primary decay of the liquid jet.

Actually, the first class of droplet breakup never was recorded in experiments as an independent process resulting in droplet breakup; however, this feature can be observed along with other disturbances [1]. We present this type of disturbance as a hypothesis, because the ten-fold domination of the aerodynamic force above the stability forces should result in droplet instability. Meanwhile, the typical time of oscillation development is longer than the speed relaxation time. It is remarkable that a similar mechanism of "droplet instability" had been hypothesized as an analog of nucleus decay.

Modes 2 and 3 exhibit rather distinguishable features and can be reproduced in experiments. For the case of high-speed jets, those mechanisms might occur at the final stage of a multi-stage spraying process.

Researchers are often disagreeing on this morphology classification for the stripping mechanisms described as items 4 and 5. Previously they were considered as a single mechanism due to similarity in droplet deformation and mass loss pattern [3, 4]. For example, the authors of [3] while studying the stream down the shock had found the growth of wavy disturbances on the windward side of the droplet; the wave stripping as mass transfer was mentioned, but in doubts. They also obtained the liquid velocity profile in the adjacent boundary layer in the droplet. Later this formula was used in publication [4], which developed a model of "boundary layer stripping". The authors of [3, 4] did not deal with We numbers. Our estimates of data from [3] revealed that for a water droplet with the size $d = 2.7$ mm and with Mach number $M_s = 1.3$, 1.5, and 1.7 for the shock waves, we can calculate the corresponding numbers as We = 1500, 4600, and 9500. It is seen that these conditions meet the interval of the flow mode number 5 (wave crest stripping) and this would not happen for gas-liquid jets. However, regime 4 is quite possible. That is why we insist on separation of those stripping-related flow modes in the framework of this study. The later publications [6, 7] confirmed the differentiation between the nature of those two regimes, and publication [7] found a criterion of transition between the modes.

Another approach for deep insight of the process is based not on the droplet morphology, but on analysis of physical mechanisms for gas flow impact on the liquid surface [1, 2, 7, 17–19]. This approach was in practice since 1970s [2]. This approach is not a denial of the previous (morphological) classification and it even takes the same set of ranges for We number: this is a hint to the initial hypothesis on balancing of disturbing and stabilizing forces applied to a droplet in gas stream. This approach claims existence of two key mechanisms for gas-droplet interaction, which produces all the diversity of droplet deformation. This approach assumes only three regimes. Starting from paper [2] (and continued in [17–19]), this approach sounds as follows.

Regime I of droplet breakup covers the three items of morphology classification: the physics basis is Rayleigh–Taylor instability (RT) or, as also cited in literature, the Rayleigh–Lamb–Taylor instability (RLT). This regime takes place for $10 \le We \le 40$ and $0.2 \le We/\sqrt{Re} \le 1$. Note that authors of [5] claimed that RLT mechanism works in the range $10 \le We \le 100$.

Regime II covers the modes 4 and 5 from the droplet morphology classification; this regime is defined through developing a conjugated boundary layer in liquid (mode 4) and KH instability (mode 5); it occurs under conditions $40 \le \mathrm{We} \le 10^3$ and $1 \le \mathrm{We}/\sqrt{\mathrm{Re}} \le 20$. In papers [3, 5–7, 17–19], the mode number 5 was observed up to $\mathrm{We} \sim 10^5$.

Regime III covers one item from the previous classification — the catastrophic breakup. This regime is different from the multistage mass loss (regime I) or on-going mass loss (regime II): this occurs as a single-moment fly-away of small-size fragments. By the physical mechanism, the catastrophic breakup of droplet corresponds to the Rayleigh–Lamb–Taylor instability (regime I); it occurs in powerful gas-dynamic pulses subjected to heterogeneous detonation. The authors of publications [17–19] had doubts on very existence of this regime for the high Weber numbers $10^3 \le \mathrm{We} \le 10^5$. However, the authors of the current study observed a similar (in morphology) regime in experiments with a falling droplet of ethanol in a falling air stream at We = 90 [20].

Although the morphology of droplet under different flow regimes was in focus of research, some of important characteristics like outcome dispersion and the interval of breakdown induction t_i [5] have insufficient study. It is worth to note that we have two characteristics: duration of breakup induction t_i and the time constant of velocity relaxation $\tau \sim (\rho_\mathrm{l}/\rho) \times \times (d/(uC_D))$ [8, 9]. Obviously, the spraying efficiency and its possibility are defined by the ratio of those two characteristic times. For $t_\mathrm{i} << \tau$, droplet breakup occurs at the early stage of velocity relaxation and reaches its full development, as this occurs for a natural-size droplet in the flow behind the shock [3–9]. For the opposite limiting case (at $t_\mathrm{i} >> \tau$), the droplet breakup does not occur, since the phase velocity contrast declines greatly during the time τ. Therefore, we can claim, at least four key factors that must be accounted for estimating the spraying performance in a gas jet:

— primary breakup of a liquid jet into droplets;

— secondary breakup of droplets under condition $\mathrm{We}\,(d, u) > \mathrm{We}_\mathrm{cr}$ while they enter the stream;

— period of breakup induction $t_\mathrm{i} = t_\mathrm{i}(\mathrm{We})$ for the current regime;

— relation between times $t_\mathrm{i}(\mathrm{We})$ and $\tau(\mathrm{Re})$.

The fast relaxation between velocities of two phases can be avoided in an accelerated flow or due to drastic changes of gas velocity typical in a system of jumps. That is why our paper is focused on high-speed (even supersonic) gas jets. The liquid was fed at the nozzle outlet along the gas stream axis: this allows jet spraying since liquid entering the stream. This geometry generates a coaxial jet with gas envelop and gas-liquid core. The structure of coaxial gas-liquid jet with the liquid feeding to the axis of a high-speed gas jet is a subject of the present study.

2. Parameters of gas-liquid jet

It is worth noting that the classification of interactions within the gas-liquid flow exclusively by We number is an incomplete approach: We number does not take into account the flow gradients. On the other hand, the problem of liquid break-up in a gas stream lacks the strict and definite initial conditions for primary droplet entering the main gas flow — here even an approximate description for two phases in the jet is of great value. The defining of conditions for interaction between two phases since the moment of entering of big droplets into the gas stream till reaching the final product (spray) remains an unsolved problem, and here we offer some approaches to this problem. Figure 1 shows a schematic diagram of a coaxial gas-liquid jet in the configuration accomplished in the current paper.

The studied processes occur in the two-phase core of jet *5*: this core is optically non-transparent for the entire length. Due to high concentration of liquid within the zone *5*, available tool cannot detect the process of primary or secondary droplet breakup. That is why it is unknown how the primary droplets enter the gas stream and at what We number this occurs [21]. Thus, the mechanisms of secondary breakup remain imprecise. The knowledge is slightly better when the droplets depart from the nozzle exit along the coordinate x, and the liquid concentration decreases considerably. However, at a high distance, the speed difference between phase declines to a minimum and the further refining of droplets comes to the end and the spray is near to its final state. It turns out that the final spray depends on initial factors describing the aerodynamic stress on droplets — the factors which are important and understudied. The liquid spraying in presented experiments occurs in subsonic and supersonic underexpanded jets. This type of gas jets is characterized by a set of detached shocks with typical alternation of gas acceleration and deceleration zones [22].

Whether those wave structures (cells) remain intact with the presence of liquid — this is a question unanswered among the unknown aspects of supersonic gas-liquid jets.

The knowledge on a gas-liquid jet structure is important, but more comprehensive description needs some quantitative parameters as well. What exactly characteristics of the gas-liquid jet should be studied – this is offered by two approaches (typical of academic and applied research). In problem statement for application, we first have to define the proper conditions for generating a spray with assigned parameters. To meet this challenge, we have to collect data for a wide range of parameters and then pick up the input conditions. Typically, this set of data is obtained from a series of single-type experiments with step-by-step variation of tested regimes (this is typical of academic research). However, now the problem is stated in the opposite manner: to define the final parameters of the spray for every specific case from the whole table of flow regimes. The condition of the spray can be described by a set of parameters available in the energy equation for the disperse phase. In the simplest case — without account for heat transfer and phase transitions — we take the spray energy $E(x)$ in a section x as a sum of gas work consumed for increasing the liquid surface S estimated as $E_S = S\sigma$, and the kinetic energy of flying droplets

$$E(x) = \frac{3\pi}{2} V_0 \frac{D_0^2}{d(x)} \sigma + \frac{\pi}{8} \rho_l V_l^3(x) D^2(x) \beta(x), \tag{1}$$

where V_0 is the initial velocity of liquid in a jet with the initial diameter D_0, σ and ρ_l are the surface tension coefficient and liquid density, $\beta(x)$ and $V_l(x)$ are the volumetric fraction and velocity of droplets with the diameter $d(x)$ at the distance of x from the nozzle exit, $D(x)$ is the diameter of the two-phase core of jet (Fig. 1). The size $d(x)$ and volumetric fraction $\beta(x)$ are also required for calculating the interface area when we have to account for heat transfer situation of thermal nonequilibrium between the phases.

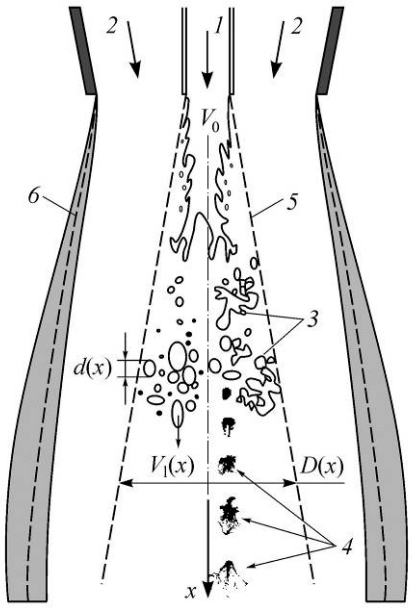

Fig. 1. Diagram of liquid jet breakup in the core of gas jet.

1 — liquid feeding with velocity V_0, *2* — air pumping, *3* – liquid jet breakup into droplets, *4* — secondary breakup of droplets, *5* — boundary of two-phase core of jet with diameter $D(x)$, *6* — mixing layer, $d(x)$ and $V_l(x)$ are droplet size and droplet velocity as function of distance x from the nozzle outlet.

The estimates obtained from expression (1) have revealed that the interface energy transfer is consumed mainly for the increase of the spray kinetic energy (the second term in (1)), but the first term is important as well. It has the parameter $d(x)$ which describes the atomization efficiency. The profile $d(x)$ is also required for estimating $\beta(x)$. Therefore, the following set of parameters for spray description in a gas-liquid flow is required: geometry parameters of main structures of the jet, like $D(x)$, dispersion profile $d(x)$, velocities of gaseous $U(x)$ and liquid $V_1(x)$ phase, and volumetric fraction of spray $\beta(x)$.

3. Experiment setup and diagnostic tools

All experiments were performed at the "Gas-liquid bench" available in ITAM SB RAS. It is constructed with the ability to create high-speed gas jets with a high content of liquid spray and operate in a wide range of modes. The general diagram of experimental setup and nozzle geometry are shown in Fig. 2. A vertical nozzle block *2* generates a coaxial gas-liquid jet suitable for optic diagnostic tools; then the jet is caught by the receiver vessel *3*, which is equipped with a draught system and a kit of mesh screens (to avoid return flow of liquid into the zone of tested flow). The nozzle block can be moved along the vertical guide within 700 mm; this helps in studying the flow structure by shifting the nozzle position while keeping the diagnostic tools *5* in steady positions. The outlet diameter of nozzle is 14 mm. The inner and outer diameters of the central pipe are 2 mm and 3 mm.

The parameters of a gas-liquid jet were measured using four optical methods. 1. PIV (Particle Image Velocimetry) was used for recording the gas flow velocity field. 2. The diffraction analyzer Malvern Spraytec was mounted for recoding spray dispersion. 3. Shadow visualization was used for recoding geometry and wave structures of the jet. 4. Laser Doppler Anemometer (LDA) measured the droplet velocity within the spray. Measurements 1 and 2 were conducted using market-available devices. Proprietary diagnostic tools created in the Lab for optic diagnostic methods in gas flows (ITAM SB RAS) were used for realization of methods 3 and 4 [23–26]. Typically, the recording of velocity field in a gas-liquid jet with a PIV tool can be performed at low concentrations of liquid in the spray (e.g., [27]), but in our case the jet

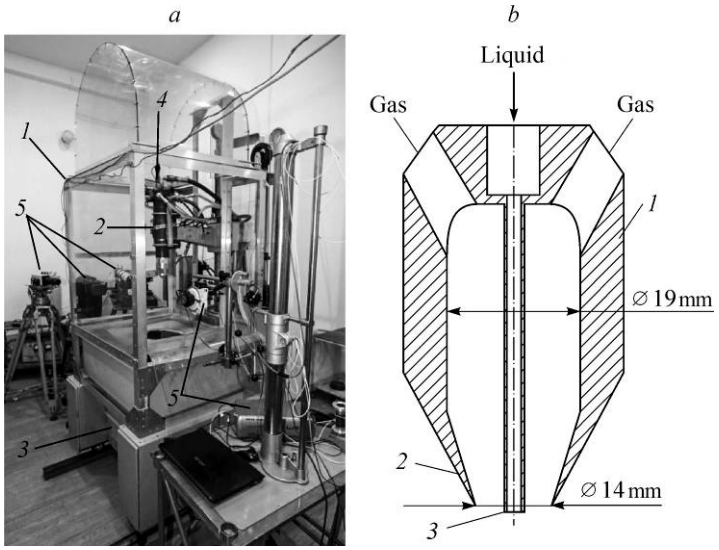

Fig. 2. General view of experimental setup "Gas-liquid testbench" (*a*) and nozzle diagram (*b*).
a: *1* — jet unit, *2* — nozzle unit, *3* — receiving tank,
4 — devices for jet parameters control, *5* — diagnostic tools;
b: *1* — casing, *2* — nozzle outlet, *3* — central pipe for liquid feeding beyond the nozzle outlet.

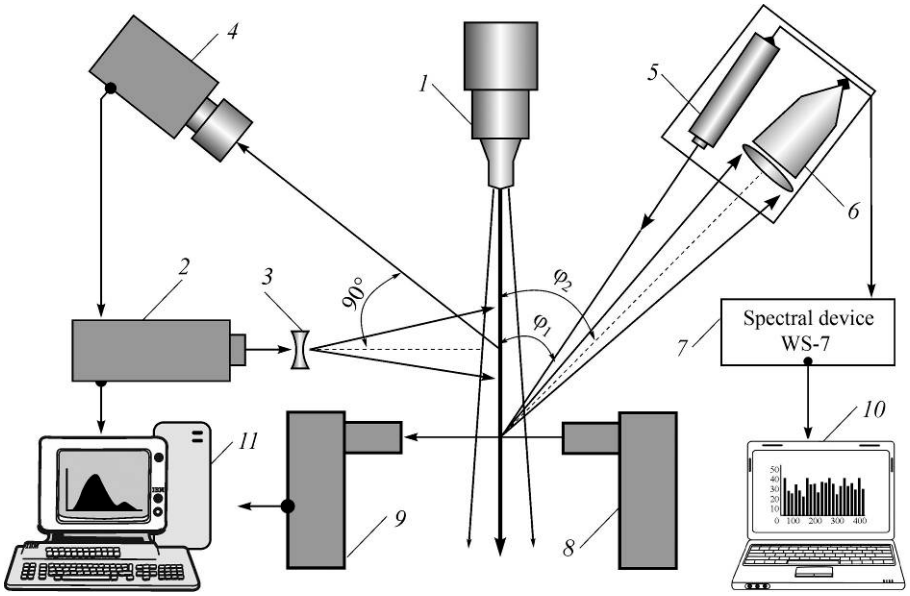

Fig. 3. Arrangement of optical tools for diagnostics.
1 — nozzle, *2–4* — elements from PIV scheme, *5–7* — laser, input slit and spectral device WS-7 in LDA system, *8* and *9* — transmitter and receiver for Malvern Spraytec, *10* — PC communicating to LDA, *11* — PC communicating to PIV.

core is not transparent and PIV method fails. Firstly, in this study, we recorded the gas velocity field in the situation without liquid (pure gas). The impact of liquid on flow structure was evaluated using the shadow visualization method (with and without liquid). The setup for shadow visualization comprises two telescopes TAL-125R with 125 mm lenses and focus distance of 1125 mm. We also used a round diaphragm with adjustable radius (normal mode) and the adaptive visualization transparent (AVT) designed for enhancing the sensitivity of this shadow method. This adaption is enough for visualization of low-speed subsonic gas jets [23].

The droplet velocity was measured with a Laser Doppler Anemometer with direct spectral analysis of frequency shift; the device was based on a multi-beam Fizeau interferometer [24–26]. The schematic of arrangement of diagnostic tools within this setup is shown in Fig. 3 (shadow analyzer is not shown). This instrumental set was used for atomization of water and dynamic of a spray in high-speed coaxial jets. The air jet was created by air flow from a convergence nozzle with the pressure ratio of prechamber to the ambient pressure NPR = = 1.5, 2, 4, and 6 at the corresponding air flowrates 33, 47, 97, and 146 g/s. The liquid flowrate was the same and kept at 45 g/s.

Figure 4 presents the shadow visualization of the near zone of supersonic underexpanded jet emitted from convergent nozzle *1* with a central pipe *2* (without and with liquid). The jet without liquid exhibits typical wavy structures of a gas jet: the barrel shock *3*, reflected shock *4*, and the Mach disk *5* at NPR = 4 (Fig. 4*a*) and NPR = 6 (Fig. 4*c*). For this configuration of nozzle, we observe not only main set of shocks, but also the tail shock *6* behind the central body *2* and its reflections. This makes the wave pattern more complicated, but the benefit is additional zones with gradients (facilitating spraying). Experiments demonstrated that this experimental setup meets the requirements to diagnostic tools formulated in section 2, except for the case of measuring the spray concentration β. However, we will show that this parameter can be evaluated indirectly from the main set of data.

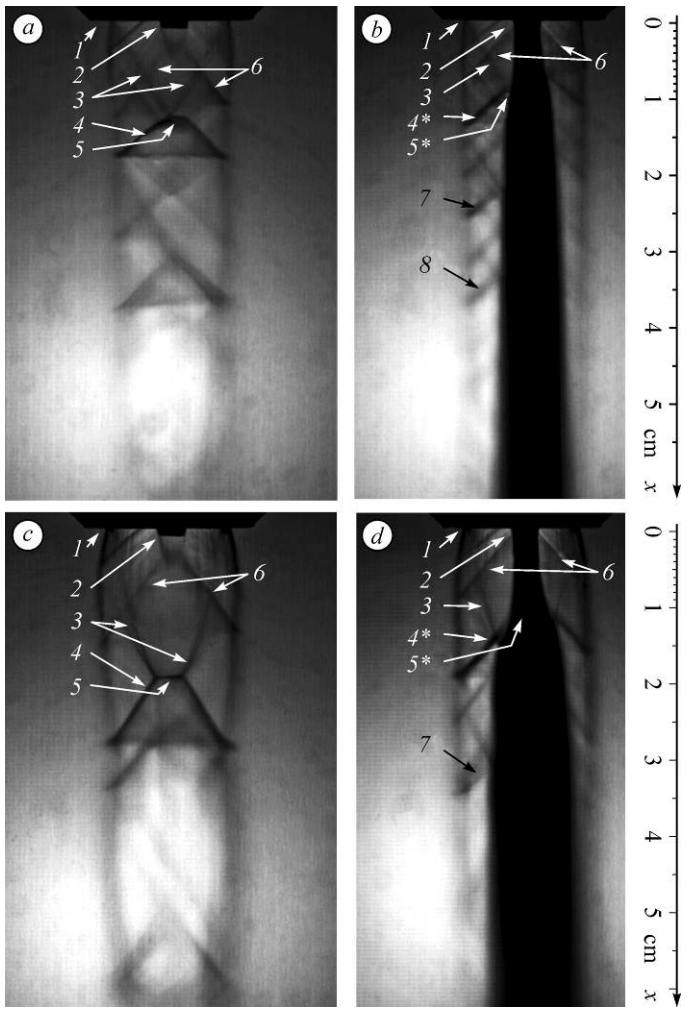

Fig. 4. Wave structure in the near-nozzle zone of supersonic underexpanded jet for regimes NPR = 4 (*a*, *b*) and NPR = 6 (*c*, *d*) for the configurations without (*a*, *c*) and with liquid (*b*, *d*).

1 — nozzle outlet, *2* — pipe for liquid feeding, *3* — barrel shock, *4* — reflected shock, *4** — reflected shock carrying liquid, *5* — Mach disk, *5** — zone of liquid jet decay, *6* — tail shock behind the central body, *7*, *8* — shocks similar to *4**.

4. Experimental results

4.1. Spray concentration in a coaxial gas-liquid jet

The spray concentration is an important characteristic of gas-liquid jet for the practical purposes and for analysis of energy balance according to (1). Since we have no special tools for measuring β, we use here the indirect estimates derived by the following method. The rules of linear optics state that for the known optic path L through the suspension of particles with diameter d, this medium would screen out a parallel light beam. This process is described by transmission index $\varphi = S_p/S$ for a limited area of CCD-matrix S, with the area S_p occupied by particles (Fig. 5*a*). At the known optical thickness of object L, the volume SL comprises N particles ($N = 6SL\beta/\pi d^3$), which can screen the area $S_p = N\pi d^2/4$, so that

$$\varphi = \frac{N\pi d^2}{4S}, \quad \text{followed by} \quad \beta = \frac{2}{3}\cdot\frac{d}{L} \text{ at } \varphi = 1. \tag{2}$$

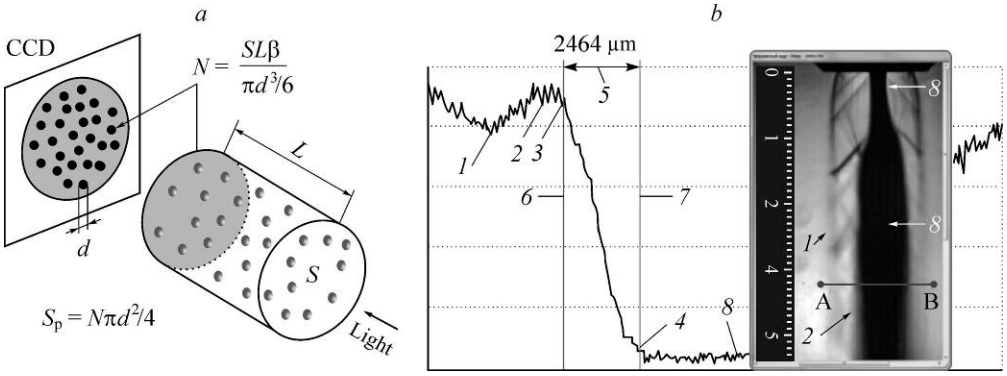

Fig. 5. Screening of a parallel light beam with aerosol (*a*)
and the light transmittance profile in the cross section of the jet in shadow images (*b*)
Segment A–B — selected section, *1* — supersonic jet boundary, *2* — gas envelope of a coaxial gas-liquid jet, *3* — boundary of a two-phase jet core, *4* — transparency boundary of a two-phase medium, *5* — measurable distance (in μm) between movable markers *6* and *7*, *8* — an opaque area.

To estimate the parameter β, we picked up the boundary of transparency for the two-phase zone ($\varphi = 1$), taken here as a defined element of the shadow image. Here the droplet concentration in this zone can be obtained if we know the average diameter of particles d and optical depth L.

The droplet size distribution for spray was analyzed by off-the-shelf device Malvern Spraytec (analysis of light angular scattering on droplets). For the case of subsonic (NPR = 1.5) and sonic (NPR = 2) jets, we observe a bimodal droplet size distribution for the jet ranging up to 150 mm (Fig. 6). The profile exhibits two size peaks (for both flow modes): ~ 35 and 300–350 μm — for the subsonic flow (NPR = 1.5), and bimodal peaks with 10 and 25 μm — for sonic jet. Note that for the sonic jet, the large droplets cannot be found in downstream zone ($x > 150$ mm). For the supersonic flow modes, the size measurement shown $d \sim 12$ μm for case NPR = 4 and $d \sim 7$ μm for NPR = 6, wherein at $x > 50$ mm there was no big difference in size distribution, while for $x < 10$ mm the liquid jet, apparently, remains intact.

The measurement of two-phase zone depth L was based on the analysis of light transmission profile on shadow images. The transmission profile (see curve in Fig. 5*b*) is a result of photo digitizing of the brightness distribution for shadow image. This task is possible with any kind of graphical code, and we used the «Image Pro» code. The optical depth L was estimated

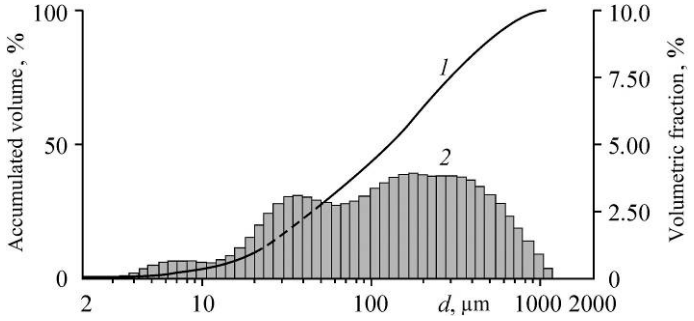

Fig. 6. Typical bimodal size distribution for a spray at NPR = 1.5
and at $x = 80$ mm.

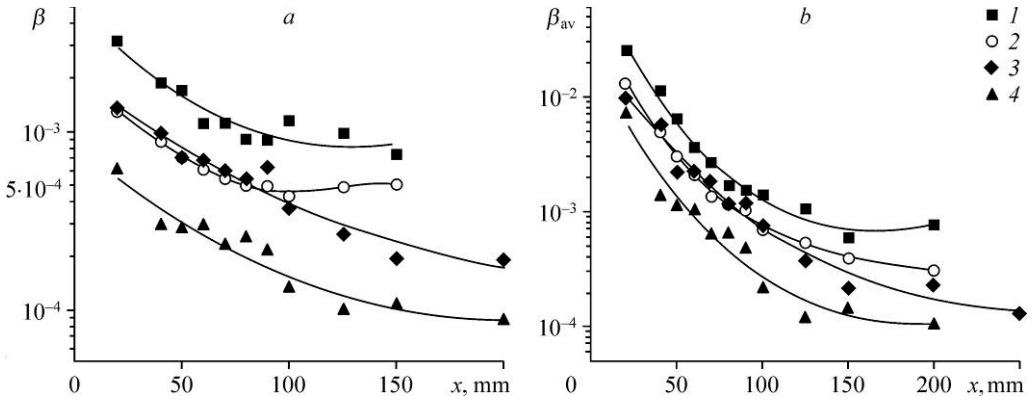

Fig. 7. Volumetric concentration in spray.

a — $\beta(x)$ at the transparency boundary of coaxial gas-liquid jet according to (2) and (3);
b — volumetric concentration averaged over jet cross section $\beta_{av}(x)$ according to (4); NPR = 1.5 (*1*), 2 (*2*), 4 (*3*) and 6 (*4*).

as a chord of the annular cross section of jet with radius $R = D/2$ under the condition that this chord is a tangent to the coaxial circumference with radius $r = R - \delta$, where r is the radius of non-transparent core of jet, δ is the distance between two movable markers *6* and *7* in Fig. 5*b*:

$$L(x) = 2\sqrt{2R\delta - \delta^2} = 2\sqrt{D(x)\delta - \delta^2}. \tag{3}$$

To estimate the uniformity of jet distribution over the jet section, we determine both the concentration β at the periphery of two-phase core of the jet and the concentration β_{av} averaged over cross section. This value is estimated from the liquid flux balance: at the known input flowrate Q_0 into the stream (in this paper, $Q_0 \approx 4.5\cdot10^{-5}$ m^3/s) the average concentration of spray β_{av} in any jet cross section with diameter of $D(x)$ is the following:

$$\beta_{av} = \frac{4}{\pi}\cdot\frac{Q_0}{D^2(x)V(x)}, \tag{4}$$

where $V(x)$ is the spray particle velocity in a section x recorded by LDA method. Figure 7*a* depicts the results of calculations for volumetric concentration $\beta(x)$ on the boundary of two-phase zone by formulas (2) and (3). Figure 7*b* presents the profile of average spray concentration $\beta_{av}(x)$ calculated by (4). Comparison of Figs. 7*a* and 7*b* demonstrates that two different approaches create similar profiles for spray concentration. This confirms the whole structure of flow, but the general tendency of decline along x axis for the average concentration shows that the average concentration by more than order higher than the boundary concentration up to distance $x \approx 100$ mm. The difference between the local and average concentrations testify that at the nozzle outlet, the main mass of liquid is concentrated in the jet core, and this is a supply source to the jet periphery. However, at distances $x \approx 150$–200 mm, the spray distribution over jet section becomes more uniform.

4.2. Spray dynamics in a coaxial gas-liquid jet

Keeping in mind the logarithmic scale for axis $\beta(x)$ and $\beta_{av}(x)$ in Fig. 7, we see that a drastic decline in spray concentration occurs at the initial segment of the jet. This decline of concentration (either local or average one) is completed up to $x \approx 100$ mm, but the shadow visualization (Fig. 4) does not reveal any special features in the jet position. We observe one peculiarity of flow: a maximum on the spray velocity profile (Fig. 8*a*). This spray deceleration

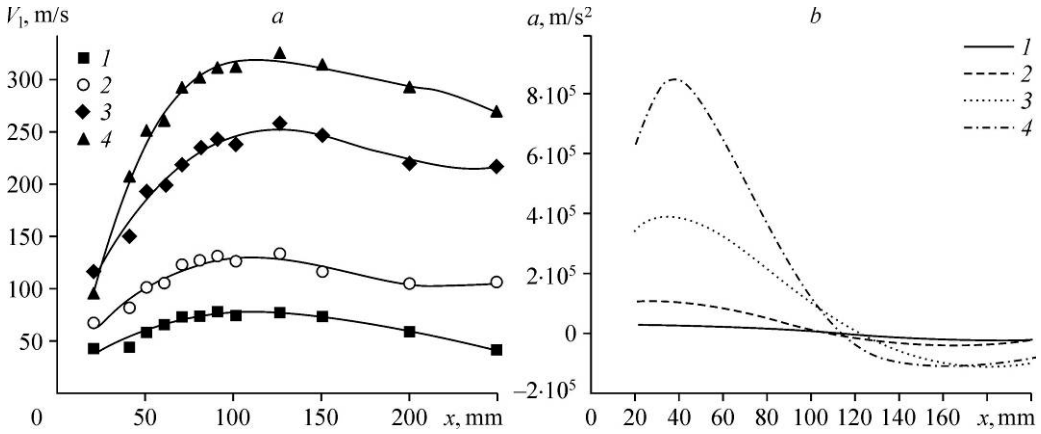

Fig. 8. Profiles for droplets velocity (*a*) and droplet acceleration (*b*) along the jet axis.
a: symbols— experiments, curves — 5-order polynomial approximation; *b*: NPR = 1.5 (*1*), 2 (*2*), 4 (*3*), and 6 (*4*).

down the maximum point can occur because of gas flow deceleration (due to losses typical of gas-only submerged jet) and because of energy loss for liquid phase atomization and acceleration of atomization products.

Figure 8*a* demonstrates that the largest acceleration for droplets takes place at the initial jet area (with the biggest difference between velocities of phases). The droplet acceleration $a(x)$ along the coordinate x was calculated by differentiation of velocity approximations $V_l(x)$, $a(x) = V_l(x)(dV_l(x)/dx)$ and plotted in Fig. 8*b*. For all tested flow modes, we observe a gas-liquid jet with the maximal velocity of spray $V_{l\,\max}$ occurring at distance of 7–8 scales (i.e., nozzle diameter) and with a maximal droplet acceleration $a_{\max}$ at the distance of 2–3 diameters. We expect that the secondary atomization is most productive in the zone of $a_{\max}$. The maximal droplet acceleration/deceleration is observed for supersonic flow modes: the deceleration can be up to $\sim -10^5$ m/s^2 at the distance of more than 10 diameters.

Thus, the measured liquid phase velocity profile allows evaluating the droplet acceleration in gas flow; which, in turn, helps in calculating the droplet size (with a sphericity assumption). Indeed, from the droplet motion equation after entering the gas flow, we can obtain the relation between the droplet diameter $d(x)$ and the acceleration $a(x)$ through this formula [8, 9]:

$$d(x) = \frac{3}{4} C_x \frac{\rho_g}{\rho_l} \cdot \frac{\left(U_g(x) - V_l(x)\right)^2}{a(x)}, \tag{5}$$

where ρ_g and ρ_l are the densities of gas and liquid, $U_g(x)$ and $V_l(x)$ are the velocity profiles for gas and liquid flows along the jet, C_x is the aerodynamic drag coefficient for the droplet. Note here that coefficient C_x for a droplet [8, 9], because of droplet deformation and mass loss can be very different from a case of solid sphere C_D [22]. According to [8, 22], we can take $C_x \approx 2C_D \sim 1–1.5$ for sonic and supersonic speeds.

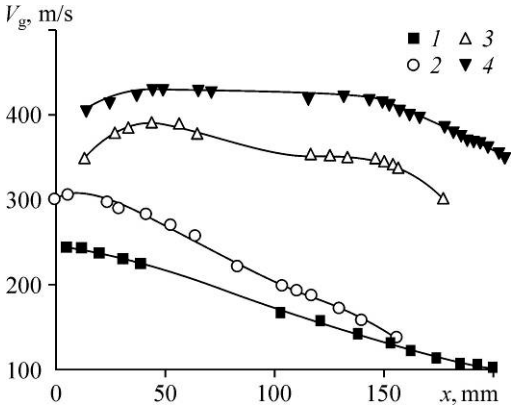

Fig. 9. Gas velocity profile at the jet axis (PIV).
Symbols — experiment, curves — 5th order polynomial approximation;
NPR = 1.5 (*1*), 2 (*2*), 4 (*3*), and 6 (*4*).

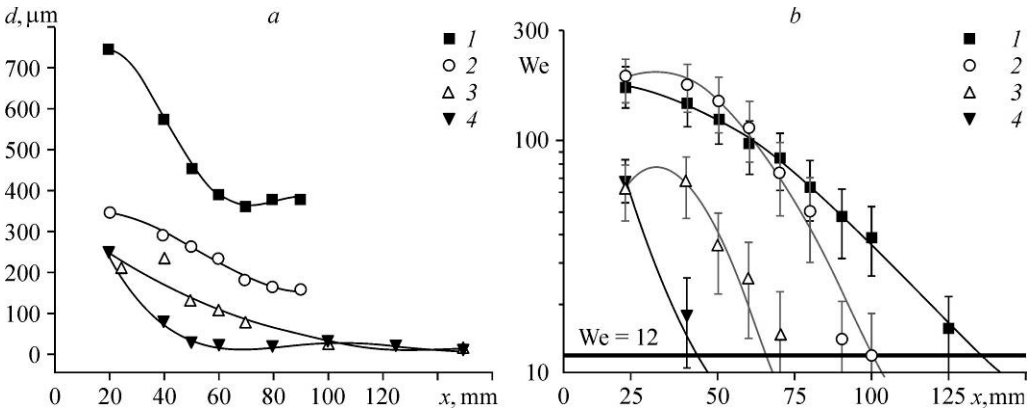

Fig. 10. Average droplet size vs. axis coordinate calculated by (5) (*a*), and Weber numbers for droplets with sizes plotted in Fig. 10*a*, in a coaxial jet (*b*).
Solid horizontal line in Fig. 10*b* is the low margin for Weber numbers (We = 12) required for aerobreakup of droplets, curves — 5th order polynomial approximation;
NPR = 1.5 (*1*), 2 (*2*), 4 (*3*), and 6 (*4*).

The experimental data on gas velocity $U_g(x)$ measured with PIV tool and used in formula (5) is plotted in Fig. 9.

The atomization results according to (5) are plotted in Fig. 10*a*. The tendency for We during acceleration and breakup the droplets along the jet is shown in Fig. 10*b*. Here Weber number We < 12 are not plotted being considered as non-physical values for further decay of droplets; meanwhile, the points above the critical We number indicate the length of zone with expectancy of efficient droplet breakup.

5. Discussion of results

Here we present a short analysis of results. First, we should review the measurement accuracy. The LDA method for measuring the dispersed phase velocity has the accuracy $\Delta V_l/V_l \approx$ ≈ 5 %, the gas velocity was measured with PIV tools with the error about $\Delta u/u \approx 10$ %. The Malvern device offers the data on particle size with accuracy $\Delta d/d \approx 5$ %, and the concentration measurements were performed with accuracy ~ 10 %. The accuracy in calculating We number is plotted in Fig. 10*b*, so the presented data would answer most of questions about the gas-droplet jet structure and mechanisms of secondary droplet breakup.

In part 2, we formulated two key questions about the flow of saturated gas-liquid jets. The first point is defining the conditions of interaction between phases since the moment of droplet entering the main stream up to the final state of spray. Since we lack the direct observations on primary breakup of the jet, all conclusions on secondary droplet breakup are founded on estimates for We number (derived from measurement of spray size and velocities of two phases). The range of We number for the case of subsonic jets (20 < We < 200, Fig. 10*b*) indicates that we face a Rayleigh–Taylor instability (RT) (bag breakup, bag-and-stamen breakup) or the mode of boundary layer stripping. For the supersonic modes of gas-liquid jet, the range for We number is rather narrow (15 < We < 70); this corresponds to Rayleigh–Taylor instability. It is known that those modes develop in two stages. This results in bimodal distribution of droplet size. The low Weber numbers (We < 70) of primary droplets occurring during supersonic flow modes can be explained by small sizes of droplets during primary breakup of liquid jet (Fig. 10*a*).

According to data in Fig. 10*b*, for flow with NPR = 1.5, the droplet breakup occurs at the length up to x = 100–120 mm (7–8 diameters), for NPR = 2, the breakup occurs only up to x = 80–90 mm (5–6 diameters), and for supersonic flow regimes the process, of atomization is completed at the distance of 50–70 mm (4–5 diameters). Comparison of droplet sizes estimated by formula (5) with experimental direct data (readings of Malvern device) have

demonstrated good agreement between two approaches for all flow modes. This means that the dynamic model is suitable for estimating the spray droplet size.

As for the second question from part 2 of this paper about conservation of wave structures (cells) in presence of liquid – the results have ambiguous interpretations. Figure 4 demonstrates that the wave structure in presence of liquid (in the transparent zone) is slightly distorted as compared to gas-only jet, but there lacks any quality difference. All key structures of underexpanded jet — input and reflected shocks — are observed. The zone of their overlapping (physically a "triple point") shows exactly the position of the direct shock — "Mach disk" — for pure gas flow. For two-phase jet core, this is an indirect indication of existence of a "third" shock originating from the triple point. There exists one more feature of back boundary of the first cell: the drastic expansion of two-phase zone of jet after flow deceleration; the same occurs on the Mach disk in supersonic underexpanded pure-gas jet. Therefore, with the involvement of liquid, the cell-like structure of jet retains (at least in the near wake), even if the boundary of the first cell may be not a flat localized shock. For the problem of efficient atomization of liquid, it is important to retain the gradient-like structure of a supersonic underexpanded jet (of any kind).

Conclusion

Experimental study was focused on coaxial gas-liquid jets with a central feeding of liquid at the outlet of a confusor-type nozzle with flow modes NPR = 1.5, 2, 4, and 6. The paper offers energy balance approach in choosing the physical parameters for total description of isothermal gas-liquid flows. The following parameters were studied: geometry of two-phase zone of jet, profiles of gas velocity and liquid velocity, droplet size, and spray concentration. For the first time, we provided the comprehensive and simultaneous measurements of droplet velocity and droplet sizes in a high-speed gas-liquid flow at a high concentration of liquid phase. Measurements demonstrated the sprays with bimodal droplet size distribution. We offered the method for evaluating the liquid concentration at the boundary of two-phase core of the jet using the shadow visualization method. Experiments measured the spray concentration averaged over gas-liquid jet cross section. It was demonstrated that at the initial part of jet, the main mass of liquid is transported within the jet core. However, at the distances about ten diameters, the spray concentration equalizes over cross section. The paper offers a method for estimating the droplet sizes from their acceleration in high-speed gradient-like flows. The gas-liquid flow was characterized by droplet size and We number from the moment of primary breakup till the final spray. The role of "bag breakup" mechanisms for generating a bimodal droplet size distribution was demonstrated. Experiments have shown that for the near wake of the supersonic underexpanded jet characterized by NPR = 4 and 6 and for the relative flow rates of liquid and gas equal 0.5 and 0.3, correspondingly, the flow retains its gradient nature.

Nomenclature

NPR — (Nozzle Pressure Ratio) ratio of pressure in nozzle prechamber to atmospheric pressure,
x — coordinate along the jet axis with countdown from the nozzle outlet,
$D(x)$ — diameter of two-phase core of jet along coordinate x,
D_0 — initial diameter of liquid jet,
V_0 — initial liquid velocity at the nozzle outlet,
$V_1(x)$ — approximation of droplet velocity along x,
$U_g(x)$ — approximation of gas velocity along x,
d_0 — initial diameter of droplet,
d — current midel diameter of droplet,
ρ, u — density and velocity of gas,
ρ_l, u_l, μ_l — density, velocity, and dynamic viscosity of liquid,
σ — surface tension of liquid,
$\beta(x)$ — volumetric concentration of spray at the boundary of transparency as a function of x,
$\beta_{av}(x)$ — averaged volumetric concentration of spray in section x,
C_x — drag coefficient of a droplet,
C_D — drag coefficient of a solid sphere,
$\tau \sim (\rho_l/\rho)(d/(uC_x))$ — time constant for velocity relaxation of droplet,
t_i — period of induction for droplet breakup,
$\mathrm{We} = \rho(u - V_1)^2 d/\sigma$ — Weber number,
$\mathrm{Re} = \rho(u - V_1) d/\mu$ — Reynolds number,
L — optical path at the boundary of transparency of two-phase zone,
φ — relative light refraction index for two-phase medium,
$a(x)$ — profile of droplet acceleration along x.

References

1. **B.E. Gelfand,** Droplet breakup phenomena in flows with velocity lag, Progress Energy Combustion. Sci., 1996, Vol. 22, P. 201–265.
2. **A.A. Borisov, B.E. Gelfand, M.S. Natanzon, and D.M. Kosov,** Droplet breakup regimes and criteria for their existence, J. Engng, 1981, Vol. 40, No. 1, P. 44–49.
3. **O.G. Engel,** Fragmentation of waterdrops in the zone behind an air shock, J. Research of the National Bureau of Standards, 1958, Vol. 60, No. 3, P. 245–280.
4. **A.A. Ranger and J.A. Nicholls,** Aerodynamics shattering of liquid drops, AIAA J., 1969, Vol. 7, No. 2, P. 285–290.
5. **M. Pilch and C.A. Erdman,** Use of breakup time data and velocity history data to predict the maximum size of stable fragments for acceleration-induced breakup of liquid drop, Int. J. Multiphase Flow, 1987, Vol. 13, P. 741–757.
6. **V.M. Boiko, A.N. Papyrin, and S.V. Poplavskii,** Dynamics of droplet breakup in shock waves, J. of Applied Mechanics and Technical Physics, 1987, Vol. 28, No. 2, P. 263–269.
7. **V.M. Boiko and S.V. Poplavski,** Experimental study of two types of stripping breakup of the drop in the flow behind the shock wave, Combustion, Explosion, and Shock Waves, 2012, Vol. 48, No. 4, P. 440–445.
8. **V.M. Boiko and S.V. Poplavski,** Particle and drop dynamics in the flow behind a shock wave, Fluid Dynamics, 2007, Vol. 42, No. 3, P. 433–441.
9. **V.M. Boiko and S.V. Poplavski,** On the dynamics of drop acceleration at the early stage of velocity relaxation in a shock wave, Combustion, Explosion, and Shock Waves, 2009, Vol. 40, No. 2, P. 198–204.
10. **K. Yu. Arefyev, A. N. Prokhorov, and A.S. Saveliev.** Study of the breakup of liquid droplets in the vortex wake behind pylon at high airspeeds, Thermophysics and Aeromechanics, 2018, Vol. 25, No. 1, P. 55–66.
11. **Yu.A. Lozhkin, D.M. Markovich, M.A. Pakhomov, and V.I. Terekhov,** Investigation of the structure of a polydisperse gas-droplet jet in the initial region. Experiment and numerical simulation, Thermophysics and Aeromechanics, 2014, Vol. 21, No. 3, P. 293–307.
12. **V.A. Arkhipov, V.M. Boiko, V.D. Goldin, E.A. Maslov, S.E. Orlov, S.V. Poplavskiy, I.K. Zharova, and A.S. Usanina,** Mathematical modelling of the liquid atomization process by cocurrent gas flow, IOP Conf. Series: Materials Sci. and Engng., 2016, Vol. 124, No. 1, P. 012076-1–012076-6.
13. **H.S. Couto, J.A. Carvalho, and Jr.D. Bastos-Netto,** The spider-jet atomizer: an evolution of the y-jet atomizer concept, IV Asian — Pacific Intern. Symp. of Combustion and Energy Utilization, 1997, P. 310–315.
14. **J.A. Schetz, P.M. Hewitt, and M. Situ,** Transverse jet breakup and atomization with rapid vaporization along trajectory, AIAA J., 1985, Vol. 23, No. 3, P. 596–607.
15. **G.M. Faeth,** Structure and atomization properties of dense sprays, in: Int. Symp. Combustion. Pittsburgh, PA: Combustion Institute, 1990, P. 1345–1352
16. **J.C. Lasheras and E.J. Hopfinger,** Liquid jet instability and atomization in a coaxial gas stream, Annual Rev. Fluid Mech., 2000, Vol. 32, P. 275–308.
17. **T.G. Teofanous and G.J. Li,** On the physics of aerobreakup, Phys. Fluids, 2008, Vol. 20, P. 052103-1–052103-14.
18. **T.G. Theofanous, V.V. Mitkin, C.L. Ng, C.H. Chang, X. Deng, and S. Sushchikh,** The physics of aerobreakup. II. Viscous liquids, Phys. Fluids, 2012, Vol. 24, P. 022104-1–022104-39.
19. **V.V. Mitkin and T.G. Theofanous,** The physics of aerobreakup. IV. Strain-thickening liquids, Phys. Fluids, 2017, Vol. 29, P. 122101-1–122101-10.
20. **S.V. Poplavski, V.M. Boiko, O.A. Gobyzov, M.N. Ryabov, and A.V. Bilsky,** Experimental study of the breakup of microdrops and drops of natural size in gradient flows, in: AIP Conf. Proceedings, 2018, Vol. 2027, Iss. 1, P. 020003-1–020003-7.
21. **L.P. Hsiang and G.M. Faeth,** Drop properties after secondary breakup, Int. J. Multiphase Flow, 1993, Vol. 19, No. 5, P. 721–735.
22. **V.M. Boiko, V.I. Zapryagaev, A.A. Pivovarov, and S.V. Poplavski,** Correction for PIV data for digital recovery of gas velocity in a supersonic subexpanding jets, Combustion, Explosion, and Shock Waves, 2015, Vol. 51, No. 5, P. 587–596.
23. **V.M. Boiko, A.M. Orishich, A.A. Pavlov, and V.V. Pikalov,** Methods for Optical Diagnostics in Aerophysical Experiments, ed.by V.M. Fomin, NSU Publ., Novosibirsk, 2009.
24. **S.V. Poplavski, V.M. Boiko, and A.U. Nesterov,** On the peculiarities of LDA method in two-phase flows with high concentration of particles, in: AIP Conf. Proceedings, 2016, P. 030016-1–030016-6.
25. **V.M. Boiko and S.V. Poplavski,** The complex of optical methods for study of gas-liquid jets, in: AIP Conf. Proceedings, 2017, Vol. 1893, P. 030002-1–030002-6.
26. **V.M. Boiko, A.U. Nesterov, S.V. Kondratev, A.A. Morozov, and A.K. Potekhin,** Laser Doppler anemometer based on the Fizeau interferometer, in: AIP Conf. Proceedings, 2017, Vol. 1893, P. 020015-1–020015-7.
27. **V.I. Terekhov, D.Yu. Starodumova, and K.A. Sharov,** PIV measurement of mean and pulsating velocities in a gas-droplet jet with low concentration of dispersed phase, Thermophysics and Aeromechanics, 2008, Vol. 15, No. 3, P. 401–407.